Research Article | Vol. 25, No. 14 | 10 Jul 2017 | OPTICS EXPRESS 16761
Optics EXPRESS

Compact photoacoustic module for methane detection incorporating interband cascade light emitting device

HUADAN ZHENG,[1,2,3,7] MINHAN LOU,[1,7] LEI DONG,[1,2,3,] HONGPENG WU,[2,3] WEILIN YE,[1] XUKUN YIN,[2,3] CHUL SOO KIM,[4] MIJIN KIM,[5] WILLIAM W. BEWLEY,[4] CHARLES D. MERRITT,[4] CHADWICK L. CANEDY,[4] MICHAEL V. WARREN,[6] IGOR VURGAFTMAN,[4] JERRY R. MEYER,[4] AND FRANK K. TITTEL[1]

[1]*Department of Electrical and Computer Engineering, Rice University, 6100 Main Street, Houston, TX 77005, USA*
[2]*State Key Laboratory of Quantum Optics and Quantum Optics Devices, Institute of Laser Spectroscopy, Shanxi University, Taiyuan 030006, China*
[3]*Collaborative Innovation Center of Extreme Optics, Shanxi University, Taiyuan 030006, China*
[4]*U.S. Naval Research Laboratory, Washington DC 20375, USA*
[5]*Sotera Defense Solutions, Inc., Crofton MD 21114, USA*
[6]*ASEE Fellow at U.S. Naval Research Laboratory, Washington DC 20375, USA*
[7]*These authors contributed equally to this paper.*
[8]*donglei@sxu.edu.cn*
[9]*lei.dong@rice.edu*

Abstract: A photoacoustic module (PAM) for methane detection was developed by combining a novel 3.2 μm interband cascade light emitting device (ICLED) with a compact differential photoacoustic cell. The ICLED with a 22-stage interband cascade active core emitted a collimated power of ~700 μW. A concave Al-coat reflector was positioned adjacent to the photoacoustic cell to enhance the gas absorption length. Assembly of the ICLED and reflector with the photoacoustic cell resulted in a robust and portable PAM without any moving parts. The PAM performance was evaluated in terms of operating pressure, sensitivity and linearity. A 1σ detection limit of 3.6 ppmv was achieved with a 1-s integration time.

OCIS codes: (280.3420) Laser sensors; (300.6340) Spectroscopy, infrared; (140.5965) Semiconductor lasers, quantum cascade.

References and links

1. M. W. Sigrist, "Trace gas monitoring by laser photoacoustic spectroscopy and related techniques (plenary)," Rev. Sci. Instrum. **74**(1), 486–490 (2003).
2. A. Miklós, P. Hess, and Z. Bozóki, "Application of acoustic resonators in photoacoustic trace gas analysis and metrology," Rev. Sci. Instrum. **72**(4), 1937–1955 (2001).
3. Y. Cao, W. Jin, H. L. Ho, and J. Ma, "Miniature fiber-tip photoacoustic spectrometer for trace gas detection," Opt. Lett. **38**(4), 434–436 (2013).
4. Z. Wang, Q. Wang, J. Y. L. Ching, J. C. Y. Wu, G. F. Zhang, and W. Ren, "A portable low-power QEPAS-based CO_2 isotope sensor using a fiber-coupled interband cascade laser," Sensor. Actuat. Biol. Chem. **246**, 710–715 (2017).
5. P. Patimisco, A. Sampaolo, H. D. Zheng, L. Dong, F. K. Tittel, and V. Spagnolo, "Quartz–enhanced photoacoustic spectrophones exploiting custom tuning forks: a review," Adv. Phys. **2**, 169–187 (2017).
6. Z. F. Gong, K. Chen, Y. Yang, X. L. Zhou, W. Peng, and Q. X. Yu, "High-sensitivity fiber-optic acoustic sensor for photoacoustic spectroscopy based traces gas detection," Sensor. Actuat. Biol. Chem. **247**, 290–295 (2017).
7. M. Siciliani de Cumis, S. Viciani, S. Borri, P. Patimisco, A. Sampaolo, G. Scamarcio, P. De Natale, F. D'Amato, and V. Spagnolo, "Widely-tunable mid-infrared fiber-coupled quartz-enhanced photoacoustic sensor for environmental monitoring," Opt. Express **22**(23), 28222–28231 (2014).
8. V. Spagnolo, P. Patimisco, R. Pennetta, A. Sampaolo, G. Scamarcio, M. S. Vitiello, and F. K. Tittel, "THz quartz-enhanced photoacoustic sensor for H_2S trace gas detection," Opt. Express **23**(6), 7574–7582 (2015).
9. G. Wysocki, A. A. Kosterev, and F. K. Tittel, "Influence of molecular relaxation dynamics on quartz-enhanced photoacoustic detection of CO_2 at λ=2 μm," Appl. Phys. B **85**(2-3), 301–306 (2006).

#297118 https://doi.org/10.1364/OE.25.016761
Journal © 2017 Received 31 May 2017; revised 28 Jun 2017; accepted 29 Jun 2017; published 6 Jul 2017

Optics EXPRESS

10. K. A. Simon, T. Ajtai, G. Gulyás, N. Utry, M. Pintér, G. Szabó, and Z. Bozóki, "Accuracy assessment of aerosol source apportionment by dual wavelength photoacoustic measurements," J. Aerosol Sci. **104**, 10–15 (2017).
11. T. Berer, M. Brandstetter, A. Hochreiner, G. Langer, W. Märzinger, P. Burgholzer, and B. Lendl, "Remote mid-infrared photoacoustic spectroscopy with a quantum cascade laser," Opt. Lett. **40**(15), 3476–3479 (2015).
12. R. Bernhardt, G. D. Santiago, V. B. Slezak, A. Peuriot, and M. G. González, ""Differential LED-excited resonant NO_2 photoacoustic system," Sensor. Actuat," Biol. Chem. **150**, 513–516 (2010).
13. J. Kottmann, J. M. Rey, and M. W. Sigrist, "Mid-Infrared photoacoustic detection of glucose in human skin: towards non-invasive diagnostics," Sensors (Basel) **16**(10), 1663–1677 (2016).
14. J. S. Li, W. D. Chen, and B. L. Yu, "Recent progress on infrared photoacoustic spectroscopy techniques," Appl. Spectrosc. Rev. **46**(6), 440–471 (2011).
15. L. Dong, V. Spagnolo, R. Lewicki, and F. K. Tittel, "Ppb-level detection of nitric oxide using an external cavity quantum cascade laser based QEPAS sensor," Opt. Express **19**(24), 24037–24045 (2011).
16. H. P. Wu, L. Dong, H. D. Zheng, Y. J. Yu, W. G. Ma, L. Zhang, W. B. Yin, L. T. Xiao, S. T. Jia, and F. K. Tittel, "Calibration-free fast quartz-enhanced photoacoustic spectroscopy based on beat frequency effect for continuous trace gas monitoring," Nat. Commun. **8**, 15331 (2017).
17. H. D. Zheng, L. Dong, X. K. Yin, X. L. Liu, H. P. Wu, L. Zhang, W. G. Ma, W. B. Yin, and S. T. Jia, "Ppb-level QEPAS NO_2 sensor by use of electrical modulation cancellation method with a high power blue LED," Sensor. Actuat. Biol. Chem. **208**, 173–179 (2015).
18. H. Zheng, L. Dong, A. Sampaolo, H. Wu, P. Patimisco, X. Yin, W. Ma, L. Zhang, W. Yin, V. Spagnolo, S. Jia, and F. K. Tittel, "Single-tube on-beam quartz-enhanced photoacoustic spectroscopy," Opt. Lett. **41**(5), 978–981 (2016).
19. Y. F. Ma, Y. He, L. G. Zhang, X. Yu, J. B. Zhang, R. Sun, and F. K. Tittel, "Ultra-high sensitive acetylene detection using quartz-enhanced photoacoustic spectroscopy with a fiber-amplified diode laser and a 30.72 kHz quartz tuning fork," Appl. Phys. Lett. **110**(3), 031107 (2017).
20. K. Liu, X. Guo, H. Yi, W. Chen, W. Zhang, and X. Gao, "Off-beam quartz-enhanced photoacoustic spectroscopy," Opt. Lett. **34**(10), 1594–1596 (2009).
21. S. Böttger, M. Köhring, U. Willer, and W. Schade, "Off-beam quartz-enhanced photoacoustic spectroscopy with LEDs," Appl. Phys. B **113**(2), 227–232 (2013).
22. L. Dong, C. G. Li, N. P. Sanchez, A. K. Gluszek, R. J. Griffin, and F. K. Tittel, "Compact CH_4 sensor system based on a continuous-wave, low power consumption, room temperature interband cascade laser," Appl. Phys. Lett. **108**(1), 011106 (2016).
23. Y. Zhang, W. Z. Gao, Z. Y. Song, Y. P. An, L. Li, Z. W. Song, W. Yu. William, and Y. D. Wang, ""Design of a novel gas sensor structure based on mid-infrared absorption spectrum," Sensor. Actuat. Biol. Chem. **147**, 5–9 (2010).
24. L. W. Kornaszewski, N. Gayraud, J. M. Stone, W. N. Macpherson, A. K. George, J. C. Knight, D. P. Hand, and D. T. Reid, "Mid-infrared methane detection in a photonic bandgap fiber using a broadband optical parametric oscillator," Opt. Express **15**(18), 11219–11224 (2007).
25. S. Suchalkin, G. Belenky, and M. A. Belkin, "Rapidly tunable quantum cascade lasers," IEEE J. Sel. Top. Quant. **21**(6), 125–133 (2015).
26. R. Q. Yang, "Infrared laser based on intersubband transitions in quantum wells," Superlattices Microstruct. **17**(1), 77–83 (1995).
27. I. Vurgaftman, W. W. Bewley, C. L. Canedy, C. S. Kim, M. Kim, C. D. Merritt, J. Abell, and J. R. Meyer, "Interband cascade lasers with low threshold powers and high output powers," IEEE J. Sel. Top. Quant. **19**(4), 1200210 (2013).
28. R. Q. Yang, B. H. Yang, D. Zhang, C. H. Lin, S. J. Murry, H. Wu, and S. S. Pei, "High power mid-infrared interband cascade lasers based on type-II quantum wells," Appl. Phys. Lett. **71**(17), 2409–2411 (1997).
29. I. Vurgaftman, W. W. Bewley, C. L. Canedy, C. S. Kim, M. Kim, C. D. Merritt, J. Abell, J. R. Lindle, and J. R. Meyer, "Rebalancing of internally generated carriers for mid-infrared interband cascade lasers with very low power consumption," Nat. Commun. **2**, 585 (2011).
30. I. Vurgaftman, C. L. Canedy, C. S. Kim, M. Kim, W. W. Bewley, J. R. Lindle, J. Abell, and J. R. Meyer, "Mid-infrared interband cascade lasers operating at ambient temperatures," New J. Phys. **11**(12), 125015 (2009).
31. I. Vurgaftman, R. Weih, M. Kamp, J. R. Meyer, C. L. Canedy, C. S. Kim, M. Kim, W. W. Bewley, C. D. Merritt, J. Abell, and S. Höfling, "Interband cascade lasers," J. Phys. D Appl. Phys. **48**(12), 123001 (2015).
32. L. Hildebrandt, R. Weih, M. Legge, N. Koslowski, M. Fischer, M. von Edlinger, J. Scheuermann, S. Becker, K. Rößner, W. Zeller, L. Nähle, J. Koeth, M. Kamp, and S. Höfling, "Cost-effective tunable laser gas-sensor module for high-volume applications, using DFB laser diodes in the NIR, and ICL in the MIR," IEEE Sens. J. **2016**, 1–3 (2016).
33. W. Ye, C. Li, C. Zheng, N. P. Sanchez, A. K. Gluszek, A. J. Hudzikowski, L. Dong, R. J. Griffin, and F. K. Tittel, "Mid-infrared dual-gas sensor for simultaneous detection of methane and ethane using a single continuous-wave interband cascade laser," Opt. Express **24**(15), 16973–16985 (2016).
34. C. T. Zheng, W. L. Ye, N. P. Sanchez, A. K. Gluszek, A. J. Hudzikowski, C. G. Li, L. Dong, R. J. Griffin, and F. K. Tittel, "Infrared dual-gas CH_4/C_2H_6 sensor using two continuous-wave interband cascade lasers," IEEE Photonic. Tech. L. **28**(21), 2351–2354 (2016).

Optics EXPRESS

35. S. Suchalkin, S. Jung, G. Kipshidze, L. Shterengas, T. Hosoda, D. Westerfeld, D. Snyder, and G. Belenky, "GaSb based light emitting diodes with strained InGaAsSb type I quantum well active regions," Appl. Phys. Lett. **93**(8), 081107 (2008).
36. A. A. Petuhov, N. D. Il'inskaya, S. S. Kizhaev, N. D. Stoyanov, and Yu. P. Yakovlev, "Effect of Temperature on the Electroluminescent Properties of mid-IR (λ_{max}=4.4 m) Flip-Chip LEDs Based on an InAs/InAsSbP Heterostructure," Semicond. **45**(11), 1501–1504 (2011).
37. N. C. Das, "Effect of indium mole fraction on infrared light emitting diode (LED) device performance," Phys. Status Solidi., A Appl. Mater. Sci. **208**(1), 191–194 (2011).
38. S. Suchalkin, S. Jung, G. Kipshidze, L. Shterengas, T. Hosoda, D. Westerfeld, D. Snyder, and G. Belenky, "GaSb based light emitting diodes with strained InGaAsSb type I quantum well active regions," Appl. Phys. Lett. **93**(8), 081107 (2008).
39. J. Abell, C. S. Kim, W. W. Bewley, C. D. Merritt, C. L. Canedy, I. Vurgaftman, J. Meyer, and M. Kim, "Mid-infrared interband cascade light emitting devices with milliwatt output powers at room temperature," Appl. Phys. Lett. **104**(26), 261103 (2014).
40. R. J. Ricker, A. Hudson, S. Provence, D. T. Norton, J. T. Olesberg, L. M. Murray, J. P. Prineas, and T. F. Boggess, "Dual-color InAs/GaSb cascaded superlattice light-emitting diodes," IEEE J. Quantum Electron. **51**(12), 3200406 (2015).
41. C. S. Kim, W. W. Bewley, C. D. Merritt, C. L. Canedy, M. V. Warren, I. Vurgaftman, J. R. Meyer, and M. Kim, "Improved mid-infrared interband cascade light emitting devices," to be published.
42. C. L. Canedy, C. S. Kim, M. Kim, D. C. Larrabee, J. A. Nolde, W. W. Bewley, I. Vurgaftman, and J. R. Meyer, "High-power, narrow-ridge, mid-infrared interband cascade lasers," J. Vac. Sci. Technol. B **26**(3), 1160–1162 (2008).
43. http://www.hitran.com
44. M. Wolff, S. Rhein, H. Bruhns, L. Nähle, M. Fischer, and J. Koeth, "Photoacoustic methane detection using a novel DFB-type diode laser at 3.3 μm," Sensor. Actuat. Biol. Chem. **187**, 574–577 (2013).
45. V. Wittstock, L. Scholz, B. Bierer, A. O. Perez, J. Wöllenstein, and S. Palzer, "Design of a LED-based sensor for monitoring the lower explosion limit of methane," Sensor. Actuat. Biol. Chem. **247**, 930–939 (2017).
46. C. M. Lee, K. V. Bychkov, V. A. Kapitanov, A. I. Karapuzikov, Y. N. Ponomarev, I. V. Sherstov, and V. A. Vasiliev, "High-sensitivity laser photoacoustic leak detector," Opt. Eng. **46**(6), 064302 (2007).
47. X. K. Yin, L. Dong, H. P. Wu, H. D. Zheng, W. G. Ma, L. Zhang, W. B. Yin, S. T. Jia, and F. K. Tittel, "Sub-ppb nitrogen dioxide detection with a large linear dynamic range by use of a differential photoacoustic cell and a 3.5 W blue multimode diode laser," Sensor. Actuat. Biol. Chem. **247**, 329–335 (2017).
48. T. Starecki, "Windowless open photoacoustic Helmholtz cell," Acta Phys. Pol. A **114**(6A), A211–A216 (2008).
49. L. Dong, A. A. Kosterev, D. Thomazy, and F. K. Tittel, "QEPAS spectrophones: design, optimization and performance," Appl. Phys. B **100**(3), 627–635 (2010).
50. M. Szakáll, H. Huszár, Z. Bozóki, and G. Szabó, "On the pressure dependent sensitivity of a photoacoustic water vapor detector using a novel modulation method," Infrared Phys. Technol. **48**(3), 192–201 (2006).
51. A. Foltynowicz, F. M. Schmidt, W. G. Ma, and O. Axner, "Noise-immune cavity-enhanced optical heterodyne molecular spectroscopy: Current status and future potential," Appl. Phys. B **92**(3), 313–326 (2008).

1. Introduction

Photoacoustic spectroscopy (PAS) is a widely used spectroscopic technique for trace gas detection due to its advantages of high detection sensitivity and selectivity as well as compactness of the detection module [1–5]. Laser sources from the ultraviolet (UV) to the far infrared region (FIR) have been applied to environmental monitoring, industrial process control and noninvasive medical diagnostics [6–11]. The photoacoustic transducer commonly used for sound wave detection in PAS is a microphone [12–14], a fiber tip [3, 6] or a quartz tuning fork [4, 5, 8, 15–21]. The principle of PAS is to detect the sound waves generated from the gas molecules upon absorption of the excitation radiation, whose frequency is resonant with the vibrational or rotational energy levels of the target gas molecule [2]. The fundamental vibrational or rotational absorption of molecules is more than two orders stronger in the mid-infrared (MIR) spectral region than in the near infrared (NIR) [22–24].

However, for spectroscopic-based trace gas sensing, the λ = 3-4 μm spectral range was referred to as the "mid-infrared gap" since commercially available quantum cascade lasers (QCLs) are limited to wavelengths >3.7 μm [25]. The interband cascade laser (ICL), which was invented by R. Q. Yang [26] and optimized by the U.S. Naval Research Laboratory (NRL) [27], filled the 3-4 μm gap and became an attractive laser source for the MIR region. Its benefits include much lower electrical power consumption and a longer carrier lifetime [28–31]. Room temperature, continuous wave ICLs are now commercially available [32] and have been applied

Optics EXPRESS

to trace gas detection systems based on tunable diode laser absorption spectroscopy (TDLAS) [22, 33, 34].

For some specialized spectroscopic chemical sensing applications and noninvasive analysis, broadband, incoherent radiation sources are preferred over single mode lasers due to their capability to cover a complete spectral absorption band of an analyte. Semiconductor light-emitting diodes emitting at wavelengths spanning 2-10 μm have been developed and commercialized [35–39]. Recently, interband cascade light emitting devices (ICLEDs, which are not strictly diodes) with 15 active stages reached a record continuous wave (cw) output power of ~1.6 mW when operated at T = 25 °C and I = 600 mA. However, the divergent emission from a MIR LED complicates the application of these novel light sources to spectroscopic chemical sensing.

To address this challenge in this work a miniaturized differential photoacoustic module (PAM) with two identical cylindrical resonators was designed to detect trace amounts of methane (CH_4). The PAM employed a novel, custom made ICLED with a 22-stage interband cascade active core, which emitted up to 2.8 mW of cw optical radiation at ~3.2 μm in a Lambertian profile at T = 25 °C and I = 600 mA [40]. An Al-coated concave reflector was positioned adjacent to a cylindrical resonator to enhance the effective absorption length. Because the ICLED and concave reflector both have small footprints, they could be embedded in the PAM to produce a robust and compact CH_4 detection module with no moving parts. The PAM performance was evaluated at different CH_4 concentration levels and pressures.

2. Characterization of the ICLED

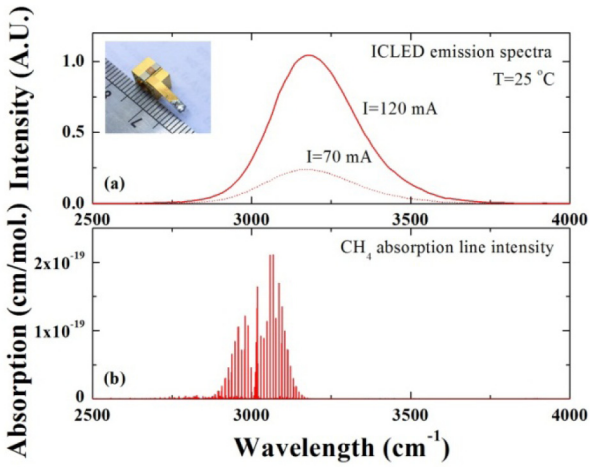

Fig. 1. (a) The ICLED emission spectra at 70 mA and 120 mA (T = 25 °C). The inset is a photograph of the ICLED; (b) CH_4 absorption band from 2500 cm^{-1} to 4000 cm^{-1}, according to the HITRAN database.

The ICLED wafer was grown by molecular beam epitaxy in a Veeco GenII molecular beam epitaxy system [41]. The structure consisted of an n^+-GaSb substrate, an n-GaSb buffer layer, a 22-stage interband cascade active core and an n^+-InAs top contacting layer. The ICLED mesa with a diameter of 400 μm was fabricated by photolithography and dry etching using of a chlorine-based inductively coupled plasma process. The mesas were metallized with Ag/Ti/Pt/Au and subsequently electroplated with Au. A circular window with 750 μm diameter was created on the substrate side for the optical emission. A custom approach was used to mount each individual device epitaxial side down on a CuW heat sink [42]. The inset of Fig. 1(a) shows a photograph of the ICLED, which has chip dimension of 6.4 × 6.4 × 5 mm^3.

Figure 1(a) shows the ICLED's normalized, continuous wave emission spectra at T = 25 °C for injection currents of 70 mA and 120 mA. The spectra were measured by a compact 1/8

Optics EXPRESS

meter monochromator (Spectral Products CM110) with a spectral resolution of 10 nm. The ICLED emission spectrum centered at 3.2 μm (~3100 cm^{-1}) covers the range 2.7-3.6 μm with a full width at half maximum of ~300 nm. This spectrum conveniently overlaps the v_3 fundamental band of CH_4, which is depicted in Fig. 1(b) from the HITRAN database [43]. The CH_4 absorption peak at 3067.3 cm^{-1} (λ ~3.26 μm) has an intensity of 2.1 × 10^{-19} cm/molecule, which is >100 times stronger than the first overtone absorption at ~1.6 μm [22, 44, 45]. Since the ICLED emission profile covers the entire v_3 fundamental band of CH_4, a high detection sensitivity can be expected.

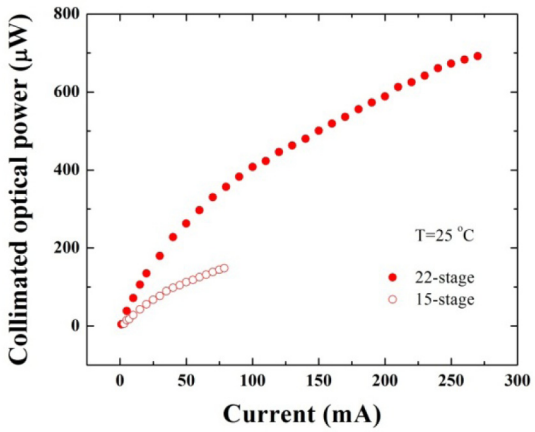

Fig. 2. Comparison of the output power from the 22-stage ICLED with that from an earlier 15-stage device (processed with the same mesa diameter of 400 μm for the study reported in [38]) as a function of injection current. Both results represent the power collected following collimation by an aspheric lens, which is less than the total power emitted in a Lambertian profile.

Figure 2 illustrates the collimated ICLED output power for different injection current levels, as measured by a power meter (Ophir NOVA II). Shown for comparison is the analogous power vs. current for an earlier 15-stage ICLED that was processed with the same 400 μm mesa diameter for the study reported in [39]. Since both ICLEDs emit in a Lambertian divergence profile, the measured optical powers depend on the efficiency of the collection optics. A 4 mm focal length aspheric lens (Thorlabs model C036TME-E) was used to collect and collimate the ICLED emission. The aspheric lens has a clear aperture of 5 mm and is coated for antireflection in the 3-5 μm spectral range. At an injection current of 80 mA, the collimated output power of 357 μW from the 22-stage ICLED is 2.4 times higher than the power of 148 μW emitted by the 15-stage ICLED. At 260 mA the 22-stage ICLED emitted ~700 μW of collimated power, which is significantly larger than any commercially-available MIR LED products can produce. The maximum output power shown in the figure is limited by the compliance voltage of the current driver. Based on NRL's characterization of the total power emitted by the device in a Lambertian profile (up to 2.8 mW at I = 600 mA, which was obtained by dividing the collimated power by the collection efficiency) [40], at least 30% more collimated power would be produced using a different higher driver compliance voltage.

A mid-infrared laser camera (Electrophysics PV320) was used to measure the collimated spot size of the ICLED as a function of working distances as shown in Fig. 3. The hyperbola-like curve showed a beam waist with diameter 6.8 mm at a working distance of 60 mm from the ICLED collimation lens. Beyond the beam waist, the spot size increased monotonically. The inset of Fig. 3 shows a MIR camera image of the ICLED beam spot at a working distance of 110 mm with T = 25 °C and I = 120 mA.

Optics EXPRESS

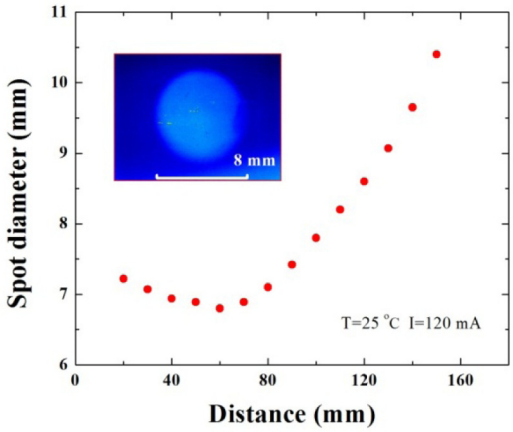

Fig. 3. Spot size of the collimated ICLED output beam as a function of working distance. The inset is an MIR camera image of the beam spot at a working distance of 110 mm, $T = 25$ °C and $I = 120$ mA.

3. Laser-embedded PAM design

A differential photoacoustic module was designed to include a photoacoustic cell, an ICLED and a reflector as illustrated in Fig. 4(a). The photoacoustic cell based on the well-known Helmholtz design [46–48] has two identical 90 mm cylindrical gas resonators with diameters of 8 mm. Two buffer chambers with lengths of 10 mm and diameters of 20 mm are placed at both ends of the gas resonators to create a total optical absorption length of 110 mm. This allows the collimated beam from the ICLED to pass through the PAM. The two buffer chambers are sealed with CaF_2 windows of diameter 25.4 mm. When the excitation radiation was modulated at the resonance frequency of the photoacoustic cell, a standing sound wave formed in the presence of an absorbing gas has its maximum acoustic pressure in the middle of the gas resonator. Therefore, two electret condenser microphones are attached to the walls in the middle of each resonator to detect the acoustic pressure. Since only one of the two gas resonators is excited by the ICLED, the gas flow noise and external acoustic disturbances are effectively suppressed by using a differential preamplifier to subtract the signal from the two microphones [47]. The ICLED is mounted on a cooled aluminum radiation plate attached to a Peltier cooler, which is embedded into the PAM. The ICLED emission is collimated and directed to the cylindrical gas resonator. An Al-coated concave reflector with $f = 50$ mm is positioned by a precision kinematic mount adjacent to the excited gas resonator. The reflector provides a double absorption pass absorption in the gas resonator in order to enhance the amplitude of photoacoustic signal. The fundamental and first longitudinal modes of the photoacoustic cell have resonance frequencies of $f_0 = 1799$ Hz and $f_1 = 5305$ Hz, with quality factors of $Q_0 = 42$ and $Q_1 = 24$, respectively. Figure 5 shows the normalized resonance curves.

Figure 4(b) shows a CAD view of the laser-embedded PAM. The ICLED and the reflector are mounted together with the photoacoustic cell resulting in a compact and robust PAM. A custom differential pre-amplifier board is attached to the surface of the photoacoustic cell. Two gas tubes with outer diameters of ~3 mm for the gas inlet and outlet are connected to the photoacoustic cell's buffer chamber. The PAM is enclosed in a protective iron enclosure with dimensions of $4 \times 4 \times 15$ cm^3.

Optics EXPRESS

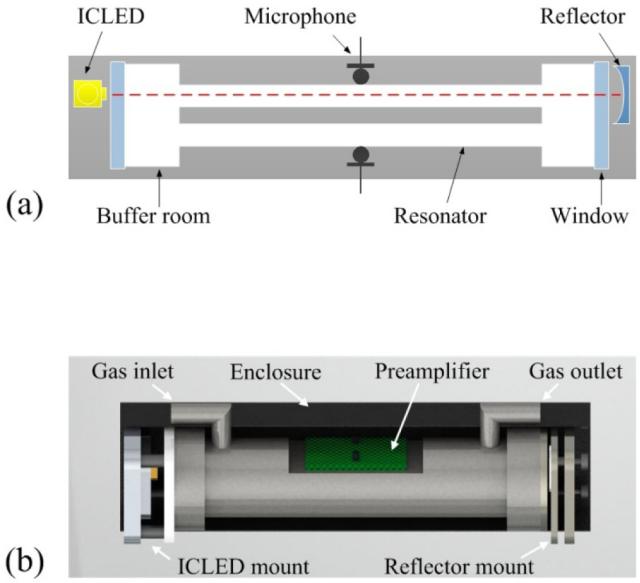

Fig. 4. (a) Schematic diagram of the differential photoacoustic cell; (b) CAD view of laser-embedded photoacoustic module (PAM).

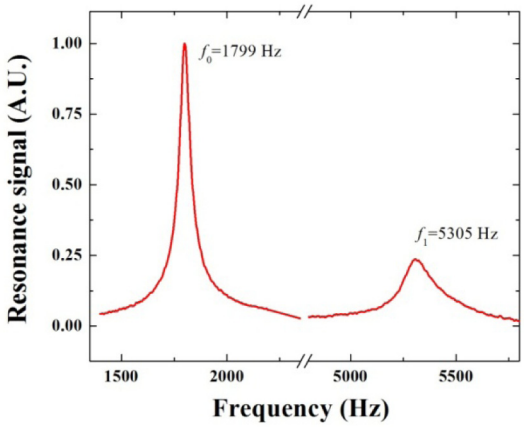

Fig. 5. Normalized fundamental and 1st longitudinal resonance curves of the photoacoustic cell.

4. Experimental set up

Figure 6 depicts the experimental setup of the photoacoustic sensor system. The temperature of the ICLED was set to 25 °C (~room temperature) by means of a temperature controller (Wavelength LDTC 0520). The ICLED offset current was provided by a laser diode driver (ILX Lightwave LDX-3232) and the modulation current with a square signal and 50% duty cycle was produced by a function generator (Stanford Research System DS345). The ICLED injection current was modulated between 3 mA and 240 mA with a frequency of 1.799 kHz, corresponding to the fundamental resonance frequency of the PAM. The photoacoustic signal detected by the microphones was first processed by the differential pre-amplifier and then fed to a lock-in amplifier (Stanford SR830) to demodulate the signal in a 1*f* mode. The time constant and filter slope of the lock-in amplifier were set to 1 s and 12 dB/otc, corresponding to a detection bandwidth of 0.25 Hz. The demodulated signal was recorded by a personal computer and the data was processed with a LabView software program.

Optics EXPRESS

A gas dilution system (Environics Inc. Model EN4000) was used to mix the 99.999% ultra-high pure N_2 and 450 ppmv CH_4/N_2 (Airgas USA, LLC) with a 2% gas analytical uncertainty. The gas pressure and mass flow in the system were controlled and monitored by a compact pressure/flow controller (MKS Instruments type 649), a vacuum pump (Hanning Elektro-werke) and a needle valve (Swagelok-316).

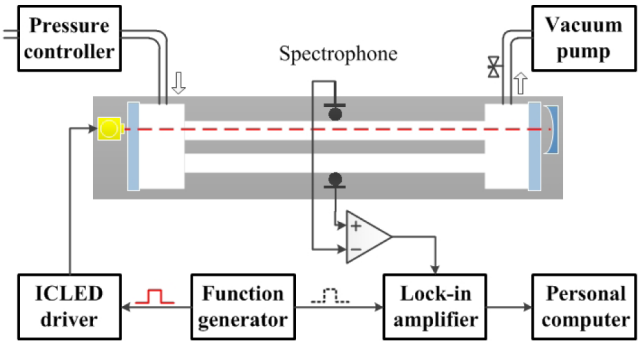

Fig. 6. Experimental setup of the photoacoustic sensor system.

5. Results and discussion

5.1 Double pass evaluation

An Al-coated concave mirror with 50 mm focal length was used to reflect the ICLED beam back through the gas channel to double the absorption length. Figure 7 shows a comparison of the photoacoustic signals obtained for single-pass and double-pass absorption. The PAS cell was filled with 450 ppmv CH_4 and the pressure was maintained at 750 Torr. The double pass effectively increased the signal amplitude from 17.7 μV to 34 μV, an increase of 92%. The signal standard deviation 1σ changed slightly from 0.16 μV to 0.18 μV indicating that no additional noise was introduced into the sensor system.

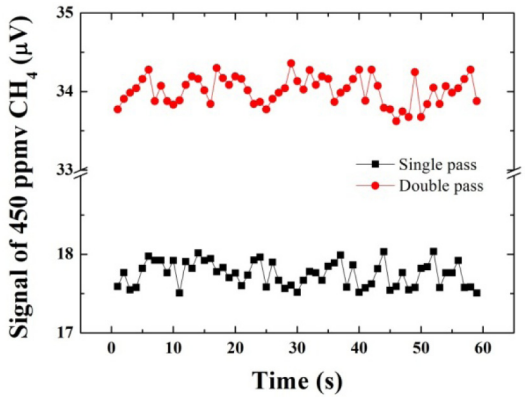

Fig. 7. Comparison of the signals for single-pass and double-pass absorption.

5.2 Pressure optimization

The photoacoustic signal amplitude is pressure dependent, which therefore requires that the pressure of the sensor system must be optimized. The 450 ppmv CH_4/N_2 gas from the cylinder was fed to the gas dilution system and the gas pressure was controlled within the range 200-800 Torr by the pressure controller and a vacuum pump. Figure 8 shows the dependence of the photoacoustic signal on gas pressure, which indicates a linear relationship since the *R*-square value for linear fitting is 0.999. Since the photoacoustic detection sensitivity is determined by

Optics EXPRESS

the pressure dependence of the microphone's sensitivity, the excited acoustic resonance of the PA cell and the V-T relaxation rate of the target gas. Both the excited acoustic resonance and V-T relaxation rate increase with total gas pressure [47, 49]. A more detailed explanation of the pressure dependence of a photoacoustic detection system can be found in [50]. In the following experiment a pressure of one atmosphere (~750 Torr) was selected to evaluate the CH_4 sensor system performance.

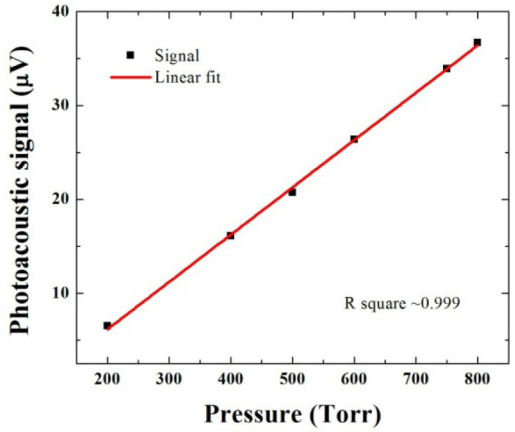

Fig. 8. Dependence of the photoacoustic signal amplitude on gas pressure.

5.3 CH_4 concentration evaluation

To evaluate the performance of the sensor system, different concentrations of the CH_4/N_2 mixture varying from 100 ppmv to 450 ppmv were fed into the PAM by means of the gas dilution system. The PAM was operated at ~750 Torr pressure and at room temperature. A period of 5 minute was allowed to mix the gas evenly and flush the sensor system completely. Sixty data points at each concentration level were acquired with a 1-s averaging time. Figure 9(a) plots the corresponding data. The signal amplitude observed for a 450 ppmv CH_4/N_2 mixture was 34 μV. Based on the 1σ standard deviation of 0.16 μV, the detection signal-to-noise ratio (SNR) is derived to be 125, which corresponds to a minimum CH_4 detection limit of 3.6 ppmv. A background offset of 14 μV was observed for pure N_2, which can be attributed to noise caused by the divergent ICLED emission. The double optical pass design increased the difficulty of the ICLED beam to clearly pass through the photoacoustic cell. The background offset cannot be removed by the differential PAM, but can be subtracted by the LabView calculation program.

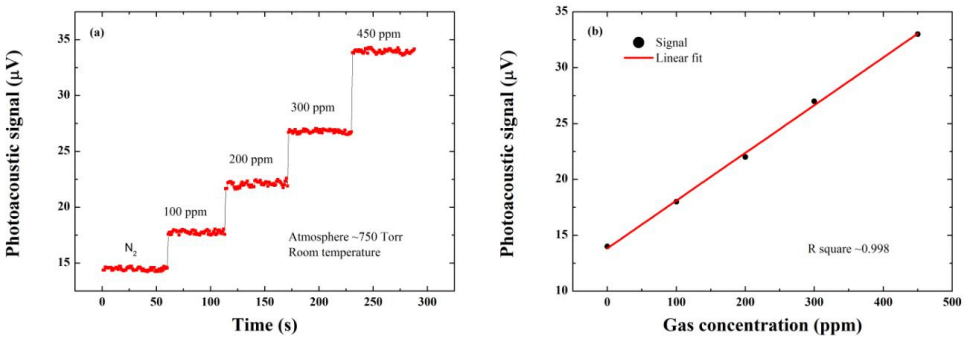

Fig. 9. (a) Photoacoustic signal at the different CH_4 concentration levels; (b) Linearity of the sensor system response.

Optics EXPRESS

The linearity of the sensor performance was verified by measuring the signal for 5 different gas concentration levels. Figure 9(b) plots the photoacoustic signals obtained when each concentration point was averaged with 60 acquired data points. Linear fitting gave an *R*-square value of 0.998, confirming the linearity of the sensor system's response to CH_4 concentrations.

6. Conclusions

In this work, we incorporated a 22-stage interband cascade LED that generates ~700 μW of collimated optical power into a compact photoacoustic module designed for sensitive CH_4 detection. Because the ICLED is unsuitable for traditional spectroscopic trace gas detection techniques such as TDLAS or cavity enhanced absorption spectroscopy (CEAS) [51], due to its divergent beam and broad spectral emission, we designed a differential photoacoustic cell that accommodates the emission profile and suppresses background noise. The ICLED's small footprint (~0.2 cm^3) makes it possible to assemble all of the PAM components into an enclosed, compact unit with no moving parts, ultra-stability, and high portability. With a 1-s integration time, the assembled system displays a minimum detection limit of ~3.6 ppmv for CH_4. Further improvement should be possible by configuring a concave Herriott cell reflector with a center hole in front of the PAS cell to enable multi-pass optical absorption. Strategies are also being explored to further enhance the ICLED output power and efficiency.

Funding

National Natural Science Foundation of China (Nos. 61622503, 61575113, 11434007); National Key Research and Development Program of China (No. 2017YFA0304203); Changjiang Scholars and Innovative Research Team in University of Ministry of Education of China (No. IRT13076), Shanxi Scholarship Council of China (No. 0011); National Science Foundation (NSF) ERC MIRTHE award and Robert Welch Foundation (No. C-0586).

Acknowledgments

The work at NRL was supported by the Office of Naval Research and Honeywell International. We also acknowledge valuable discussions with Terry Marta.